Smart Structures and Systems, *Vol. 35, No. 2 (2025) 101-113*
https://doi.org/10.12989/sss.2025.35.2.101

Multimodal data fusion damage identification method in noisy environments: A case study of cable-stayed bridges

Yue Cao*[1,2], Longsheng Bao[2], Xiaowei Zhang**[2] and Zhanfei Wang[2]

[1] *School of Civil Engineering, Shenyang Jian Zhu University, Shenyang, 110168, China*
[2] *School of Transportation and Geomatics Engineering, Shenyang Jian Zhu University, Shenyang, 110168, China*

(*Received July 17, 2024, Revised February 13, 2025, Accepted March 3, 2025*)

Abstract. To enhance the accuracy of damage detection and prevent misjudgments when applying a single damage index, we have developed a method for multivariate data fusion damage detection based on signal denoising. This approach involves fusing two modal indicators and two vehicle excitation response indicators, ultimately performing a secondary fusion of the combined indicators. A statistical noise reduction method was applied to minimize noise in the fundamental indices. A mode-based fusion index was created based on the curvature and displacement modes, whereas a fusion index based on the vehicle excitation response was generated by using the acceleration energy difference and acceleration energy-curvature difference. The Dempster-Shafer evidence theory was utilized for the secondary fusion of multiple fusion indices, leading to higher damage detection accuracy. The effectiveness of the damage identification method was confirmed by the ratio of the sub-peak value to the peak value. Moreover, numerical simulation data from a cable-stayed bridge further validated the damage detection method, showing a significant decrease in the ratio of the sub-peak value to the peak value (i.e., a reduction of 16-99%) after secondary fusion. These results demonstrate the feasibility of this method.

Keywords: cable-stayed bridge; damage detection; Dempster–Shafer evidence theory; noise reduction; statistics

1. Introduction

Bridges have a significant impact on various aspects of daily life, including the economy (Moschas *et al*. 2013). This is particularly important when the bridge is in operation. Although large-bridge engineering technologies have evolved rapidly in recent years (Torbol *et al*. 2013), bridge accidents frequently occur during operation. Thus, given the necessity to effectively guarantee the safety of people's lives and property, civil engineering researchers have begun focusing on bridge health monitoring. Owing to the long service life of bridges, their environmental conditions change over time. For instance, the load on the bridge constantly fluctuates; thus, the potential risk of damage is high. Because bridge damage typically develops from localized damage, it is difficult to detect intrinsic damage via visual inspection. The bearing capacity and durability of the bridge will be affected if the damage location is not found during improvements such as bridge repair and reinforcement. Furthermore, the accumulation of time results in accumulated damage, which leads to serious accidents, immeasurable economic losses, and a negative social impact. Therefore, research on damage detection in bridges during service periods is of great practical significance.

*Corresponding author, Ph.D. Student,
E-mail: sycy@sjzu.edu.cn
**Co-corresponding author, M.S.,
E-mail: syzxw@sjzu.edu.cn

Currently, vibration- (Yıldırım 2023) and testing-based (Daneshvar *et al*. 2023) methods for damage detection (Barros *et al*. 2023) are being widely (Jamshidi and El-Badry 2023) applied to bridges (Reynders *et al*. 2007). Mekjavic (2013) derived formulas for stiffness and mass damage indicators and employed frequencies to realize structural damage detection. Hosseinzadeh *et al*. (2016) proposed a novel approach for detecting structural damage that involves utilizing a flexibility matrix before and after the damage. They computed the differences between the columns and rows of the flexibility matrix to obtain a flexibility-difference curvature matrix. The diagonal elements of this matrix were then applied as indicators to effectively detect structural damage. Shi *et al*. (2024) proposed probabilistic and interval methods grounded in the residual force vector technique to quantify measurement uncertainties and effectively integrate them into the identification process. Zhang *et al*. (2023) proposed a damage identification method based on mobile vehicle response signals. Verified through finite element models and actual bridges. And satisfactory results were obtained.

During bridge operation, external interference factors, such as noise and temperature, inevitably affect the response of the structure (Wang *et al*. 2022). The position of the neutral axis (NA) is inevitably affected by the nonlinear temperature gradient of girders, which might mask the abnormality caused by damage. The influence of temperature can be minimized by screening the data of bridge health monitoring in different periods. However, noise cannot be avoided. In some cases, the noise may be too large, even exceeding the magnitude of the signal itself

ISSN: 1738-1584 (Print), 1738-1991 (Online)

(Li *et al*. 2024). Therefore, the noise processing are crucial for accurate damage detection. Additionally, because the level of early damage in bridges is relatively low (Sousa Tomé *et al*. 2019), relying on a single damage indicator may not provide sufficient information to accurately assess the extent of localized damage, which can potentially lead to misjudgment. Multiple damage indicators should be applied to enhance the reliability and fault tolerance of damage detection methods and prevent misjudgment.

To reduce the effects of noise in the process of damage detection, Fathi and Naghsh-Nilchi (2012) demonstrated the robustness of their method by using wavelet packet decomposition and wavelet threshold denoising. Seyedpoor and Yazdanpanah (2014) proposed a strain–energy variation method for damage detection that entails the use of static noise data. Bai *et al*. (2017) proposed a Katz fractal dimension-integrated trace-scanning fusion method for plate-like structure damage detection. This method involves the threshold denoising of the double tree complex wavelet transform, discrete decomposition of the plate vibration modes, and affine transformation preprocessing. Sohn and Law (2015) introduced the application of Bayesian methods, and their proposed damage detection method can apply the simplified analytical models and modal parameters derived from vibration testing to locate damaged areas. Chakrabarty *et al*. (2015) proposed a Bayesian method for spatial filtering and diffusion power estimation that combines reverberation and noise reduction. Building on the previous work, the authors developed a multilevel sparse Bayesian learning model to identify structural damage and implemented a sparse Bayesian learning algorithm to determine the location and extent of the suspected damaged elements. The effectiveness of this method has been validated for both single-element and multiple-location damage scenarios in a spatial grid. Although previous research on wavelets (Shelley and Liew 2013) and data fusion algorithms has demonstrated potential for noise interference reduction and recognition accuracy maximization, wavelets are most effective in situations in which the frequency range of the noise is known and the frequency bands of the signals and noise can be separated. However, the denoising effect of the wavelets is relatively weak for white noise, which is commonly encountered in practical applications. Bayesian algorithms require large amounts of data, complex calculations, and subjective probabilities for certain data (AlMutawa 2007). Therefore, further research is required to explore the practical engineering applications of these techniques (Liu *et al*. 2015). Dempster–Shafer evidence theory is an extension of Bayes theory. The calculation is simple and requires no prior probability. It can handle uncertain data well. Therefore, it is necessary to apply Dempster–Shafer evidence theory to damage identification theory (Wang *et al*. 2019). This approach helps to address the limitations of traditional methods and improves the accuracy of damage identification.

In order to address issues such as noise and misjudgements of damage. In this study, a multivariate data fusion method for damage detection based on signal denoising was developed to enhance identification accuracy and reduce noise interference. By treating the noise using noise reduction techniques, the dynamic response of a bridge can be separated from the noise. To address the problem of misdiagnosis in single damage index identification, new damage indices were constructed by combining the modal index with the moving load excitation response index. These new indices were fused by using Dempster–Shafer (D–S) evidence theory to increase the efficiency of damage detection. The effectiveness of the proposed method has been confirmed by using a finite-element example.

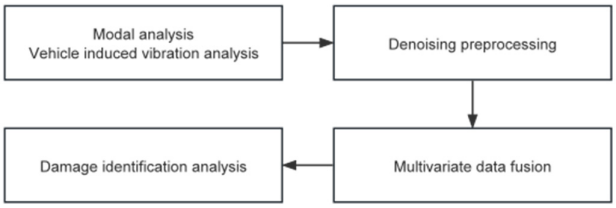

Fig. 1 Numerical framework

To summarize, the numerical framework for this study is shown in Fig. 1.

2. Data fusion theory based on noise reduction

2.1 Statistical noise reduction theory

Principal component analysis (PCA) is based on the concept of dimensionality reduction. The main objective of this study was to explain the correlation between multiple variables and a few principal components. Each principal component is a linear combination of the original variables that is designed to retain as much information as possible about the original variables; additionally, the principal components are not related to each other. Generally, PCA has two purposes: to compress and interpret the data. Using this method, complex factors can be divided into several main components, and redundant information can be eliminated to simplify the complex problem. Consequently, the information obtained is scientific and accurate, which allows the model to better reflect real-life situations. However, a portion of the original data is lost after dimensionality reduction, and the resulting principal components generally cannot be clearly interpreted, as the information represented by them is not as clear or accurate as the original data. The PCA technique was improved to mitigate information loss in data compression processes.

The interpretation of the components output by the PCA method can be inaccurate because of the incomplete information. The proposed method to rectify this is as follows. The load of the original variables on the principal components is redistributed by the rotation of the factor axis, that is, the rotation of the coordinates. For example, if PCA obtains the initial common factors F_1, F_2, ..., F_m. Factor rotation is the linear combination of the initial common factors to obtain a new set of common factors. That's F_1', F_2', ..., F_m'. The rotating factor load can more clearly indicate the importance of the factor. Make important common factors more weighted in linear combinations. Less important common factors have less weight. The modes of factor rotation are orthogonal rotation

and oblique rotation. The new common factor after orthogonal rotation is still independently orthogonal. The oblique new common factors give up the restriction that the factors are independent of each other. It can be expressed by the following formula.

$$\begin{matrix} F_1 \\ F_2 \\ \vdots \\ F_m \end{matrix} \quad \begin{matrix} \text{Factor rotation} \\ \Rightarrow \end{matrix} \quad \begin{cases} F_1{}' = d_{11}F_1 + d_{12}F_2 + \cdots + d_{1m}F_m \\ F_2{}' = d_{21}F_1 + d_{22}F_2 + \cdots + d_{2m}F \\ \vdots \\ F_m{}' = d_{m1}F_1 + d_{m2}F_2 + \cdots + d_{mm}F \end{cases} \tag{1}$$

Where ***d*** denotes the factored rotation coefficient matrix.

Thus, the load of the original variable on the common factor is polarized, and the principal components can be explained by the original variables with a large load. This process can also be used to observe the degree of hidden factor extraction from the original feature information and thus effectively eliminate noise.

For *N*-dimensional data **X**, if it is assumed that it has one column factor, **X** can be expressed as

$$X = \begin{bmatrix} X_1 \\ \vdots \\ X_n \end{bmatrix} = \begin{bmatrix} A_{11} & \cdots & A_{n1} \\ \vdots & \ddots & \vdots \\ A_{1n} & \cdots & A_{nn} \end{bmatrix} \begin{bmatrix} f_1 \\ \vdots \\ f_n \end{bmatrix} + \begin{bmatrix} \varepsilon_1 \\ \vdots \\ \varepsilon_n \end{bmatrix} \tag{2}$$

where $f_1, f_2, \ldots, f_n$ denote n column factors of data $\boldsymbol{X}$; A_{pj} is the load of the p-th common factor f_p on the j-th component x_j of $\boldsymbol{X}$; ε_j is the special factor of x_j.

Simplify the above expression into a mathematical model, which can be written as

$$X = Af + \varepsilon \tag{3}$$

where ***A*** denotes the factored load matrix. Then, the mathematical expression of the special factor is

$$\varepsilon = Af - X \tag{4}$$

If the common factor of each component in the original data is calculated, the component of the common factor in the original data can be eliminated. Noise exists in all of the dynamic response data and belongs to the common factor category. Therefore, special factors were extracted to reduce the impact of noise factors.

2.2 Data fusion theory

The D–S evidence theory was originally proposed by Dempster and subsequently developed by Shafer. This theory solves the uncertainty problem by determining the basic probability assignment of uncertain events and combining specific rules. It belongs to the artificial intelligence category and was first applied to expert systems with the ability to process uncertain information. As an uncertainty reasoning method, the main characteristic of evidence theory is that it satisfies conditions that are weaker than those of Bayesian probability theory, as it has the ability to directly express uncertainty and unknowns.

This theory has been applied for the detection of damage in engineered structures and has allowed us to assign the probability of the damage detection results of multiple independent sensors by fusing multiple sensor datasets based on operational rules.

Assume that A is the damage-identification framework of a cable-stayed bridge or assumed space.

$$\theta = \{\theta_1, \theta_2, \cdots, \theta_n\} \tag{5}$$

where $\theta_i (i = 1,2,\cdots,n)$ denotes the i-th element of the cable-stayed bridge. Its power set 2^θ is a probability mass function that has been allocated to the identification framework, where $0 \leq \text{mass} \leq 1$, $mass(\varphi) = 0$, and $\sum_{A\subseteq\theta} mass(A) = 1$.

When there are n sensors, n mass functions exist. The operating rules for these n mass functions are as follows

$$\begin{aligned} &(mass_1 \oplus mass_2 \cdots \oplus mass_n)(A) \\ &= \frac{1}{k} \sum_{A_1 \cap A_2 \cdots \cap A_n = A} mass_1(A_1)\, mass(A_2) \cdots mass(A_n) \end{aligned} \tag{6}$$

where $A_1, A_2, \cdots, A_n \subseteq \theta$ and $k = \sum_{A_1 \cap A_2 \cdots \cap A_n \neq \varphi} mass_1(A_1) mass_2(A_2) \cdots mass_n(A_n)$.

Where k is the normalization coefficient.

Taking into consideration the D–S evidence theory synthesis rule, the multi-sensor data fusion technique was extended to include multi-damage index data in the D–S evidence fusion strategy. The results of different damage identification indexes were fused instead of sensor data.

3. Construction of multivariate damage index

Structural health monitoring (SHM) is a critical aspect of ensuring the safety and longevity of civil infrastructure. Among various approaches to SHM, the development of robust damage indices plays a pivotal role in accurately identifying and localizing structural damage. Traditional methods often rely on single indicators, such as frequency changes or modal shapes, which may not fully capture the complexity of structural responses under varying conditions. To address this limitation, this study proposes a multivariate damage index that integrates multiple modal and response-based indicators. By leveraging the complementary strengths of different damage-sensitive features, the proposed approach aims to enhance the accuracy and reliability of damage detection in complex structures, such as cable-stayed bridges.

3.1 Mode-based damage index construction

3.1.1 Mode of displacement

The displacement mode generally contains more structural information than the frequency mode. Furthermore, the higher-order displacement mode is more sensitive to localized structural damage. These

characteristics have to be taken into account to determine the damage location in the structure.

It is generally difficult to generate high-order modes in actual engineering applications. Therefore, only the lowest-order displacement mode was used as an example for calculation and analysis. Specifically, the first-order mode was selected as the mode index.

The displacement mode difference (DMD) before and after damage to a cable-stayed bridge was considered as one of the damage indices to enable damage detection.

$$DMD = \delta_{\text{before}} - \delta_{\text{after}} \tag{7}$$

3.1.2 Mode of curvature

The curvature of a point on the girder is inversely proportional to its corresponding stiffness. Therefore, changes in the rigidity of the structure are reflected in the curvature.

Considering this, the curvature mode difference (CMD) has been used as one of the damage indices

$$CMD = \delta''_{before} - \delta''_{after} \tag{8}$$

$$\delta'' = \frac{\delta(x_{i-1}) - 2\delta(x_i) + \delta(x_{i+1})}{l_{i-1,i} l_{i,i+1}} \tag{9}$$

where $l_{i-1,i}$ is the distance from sensor *i-1* to *i* and $l_{i,i+1}$ is the distance from sensor *i* to *i*+1.

3.2 Damage index based on vehicle excitation response

The acceleration energy is defined as follows

$$E = \frac{1}{2}\sum_{i=1}^{n} m_k \left(a_i^k\right)^2 \tag{10}$$

where m_k is the mass at node *k* and a_i^k is the acceleration at moment *i* at node *k*.

Next, the characteristic function to describe the damage, i.e., *AE*, can be derived based on the acceleration energy concept and expressed as shown in Eq. (11)

$$AE_k = \sum_{i=1}^{n} \left(a_i^k\right)^2 \tag{11}$$

The difference in energy of the acceleration before and after damage was calculated. The difference in the acceleration energy curvature was calculated using the central difference method. The calculation formula for the difference in acceleration energy curvature as shown in Eq (12)

$$AE_k C_i = \frac{AE_{k_{i-1}} - 2 \times AE_{k_i} + AE_{k_{i+1}}}{h} \tag{12}$$

Where: AE_kC_i represents the acceleration energy curvature at measurement point i, AE_{ki} denotes the acceleration energy at measurement point i, and h is the distance between two adjacent measurement points.

We calculated and obtained the acceleration energy difference and AE_k rate of change. The basic probability assignment was calculated after fusion, according to the D–S evidence theory operating rules. Lastly, the fusion damage metrics were obtained.

3.3 Research methodology

Before multimodal data fusion, calculate the basic possibility assignment (BPA) for each measurement point under each indicator. Incorporating modal indices (Mi) and vehicle-induced vibration indices (Vivi). The BPA can be represented by Eq. (13). Mi is derived from the fusion of displacement mode and curvature mode data. Vivi is obtained from the fusion of acceleration energy and acceleration energy curvature. The fusion method for Mi and Vivi is also consistent with Eqs. (13), (14), and (15). The calculation process of Mi requires Eqs. (7) and (8) to determine two mass functions respectively; while the calculation process of Vivi requires Eqs. (11) and (12) to determine two mass functions respectively.

$$m_1(x_i) = \frac{\text{Mi}_i}{\sum_{i=1}^{n} \text{Mi}_i}, m_2(x_i) = \frac{\text{Vivi}_i}{\sum_{i=1}^{n} \text{Vivi}_i} \tag{13}$$

where x_i is the measuring point on the bridge; m_1 is the BPA of the modal index, and m_2 is the BPA of the vehicle

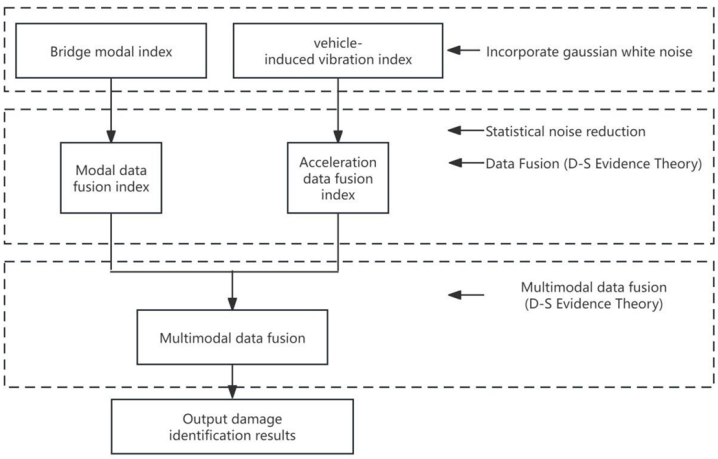

Fig. 2 Data fusion process

induced response index.

The normalization coefficient k can be represented by Eq. (14)

$$k(x_i) = m_1(x_i) \times m_2(x_i) \tag{14}$$

Multimodal data fusion results can be represented by Eq. (15)

$$m_1 \oplus m_2 = \frac{m_1(x_i) \times m_2(x_i)}{\sum_{i=1}^{n} k_i} \tag{15}$$

where $m_1 \oplus m_2$ is the results of multimodal data fusion.

Based on the above-mentioned fusion rules, the damage detection data fusion process for cable-stayed bridges was implemented as illustrated in Fig. 2.

4. Numerical verification

The main bridge is a single-tower cable-stayed bridge with an approach bridge comprising a reinforced concrete cast-in-place box girder and a prestressed concrete cast-in-place box girder. The specific span arrangement was (32.50 + 40.00 + 30.76) m + (152.00 + 48.00 + 42.00) m + 13.00 m. The (152.00 + 48.00 + 42.00) m segment represents the main bridge section, as depicted in the front view of the bridge in Fig. 3.

The main girder was of the composite type, comprising steel and prestressed concrete girders. The main beam had a double-box, double-chamber, and thin-walled section with an air nozzle. The main span was made of steel, whereas the side span was made of prestressed concrete. The joint was located 7 m away from the main pier on the main-span side. The cross-sectional view of the main beam is shown in Fig. 4.

The cable tower of the main bridge featured an arched steel structure with an elliptical curve along its central axis. The main tower stood at a height of 78.00 m above the main beam structure, inclined at an angle of 75.0°. The main beam passed through the tower, with the spacing of the cables on the main tower gradually increasing from 2.50–3.40 m from top to bottom in a sector cable formation. The dip angle of the main-span cable ranged from 24.1° to 47.7°, whereas the side-span cable dip angle varied from 45.2° to 70.6°. The stay cables were multi-strand parallel steel wire-finished cables with a mid-span cable pitch of 6.00 m and a side-span cable pitch of 3.80 m. In addition, the main girders of the central tower are connected through a rigid connection method.

4.1 Finite-element model

The finite-element cable-stayed bridge model shown in Fig. 5 was utilized for the modal and dynamic response analyses of moving loads. The total bridge length was 242 m, which was divided into 147 elements based on the actual design. The main span girder consisted of steel with an elastic modulus of $E = 2.06 \times 10^5$ MPa and Poisson's ratio of $\mu = 0.3$; it featured a Π-shaped beam section with a moment of inertia of $I = 1.21$~1.36 m^4. The main bridge back span was a reinforced concrete structure with an elastic modulus of $E = 3.45 \times 10^4$ MPa and Poisson's ratio of $\mu = 0.2$; it also had a Π-shaped I-beam section with a moment of inertia of $I = 13.88$~15.95 m^4. The supports of the model were arranged sequentially at nodes 1, 24, 50, and 148. The constraint conditions for the supports are

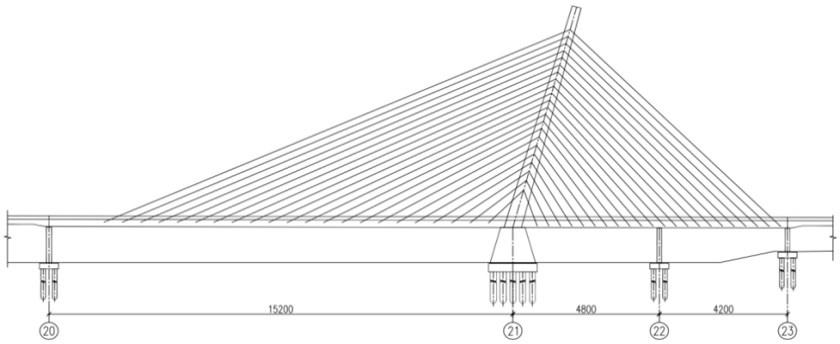

Fig. 3 Front view of main bridge section

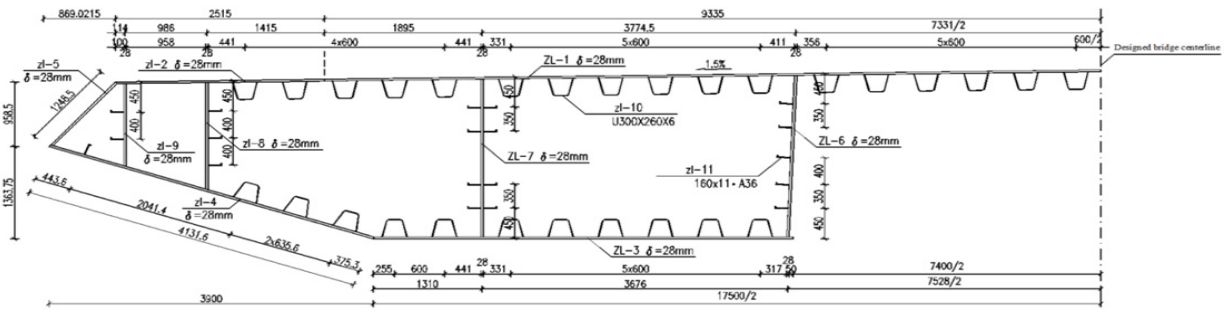

Fig. 4 Bridge cross-section

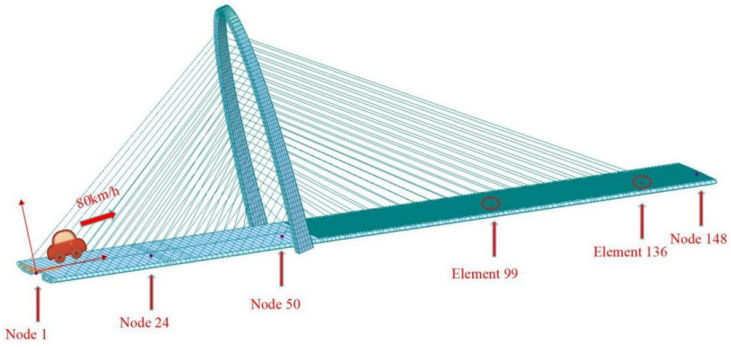

Fig. 5 Model schematic diagram

listed in Table 1. Modal analysis was conducted to extract first-order modal data, with the moving load simplified to a concentrated load of approximately 2 T and a velocity of 80 km/h. The dynamic response of the cable-stayed bridge under the action of a moving load was analyzed by determining the complete transient response. The finite-element model was loaded by using the Newmark method of time integration, which entailed applying a load to the main beam element node at each load step. Using one sensor placed under each node, the dynamic response data for each measurement point in the time history were obtained as the original data. The time for vehicles to cross the deck at 80 km/h was estimated to be 10.9 s; therefore, the data is simulated.

For this study, we assumed that, when structural damage occurs, it is only related to changes in structural stiffness. Therefore, in this study, the beam damage in the cable-stayed bridges was simulated by applying stiffness reduction. In practice, several factors influence the dynamic responses (Desjardins and Lau 2024). Given that the allowable measurement error in engineering applications is approximately 5% (Liu *et al*. 2021), we categorized 5% damage as minor damage. We also established two types of damage conditions: a single point of damage and two points of damage, as described in Table 2.

Table 1 Boundary conditions of the simulation model

Node number	Dx	Dy	Dz	Rx	Ry	Rz	Rw	Node location (unit: m)
1	0	1	1	0	0	0	0	0
24	0	1	1	0	0	0	0	42
50	1	1	1	1	1	1	0	90
148	0	1	1	0	0	0	0	242

Table 2 Simulation damage conditions

Working condition	Damage degree /%	Damage element	Damage location (unit: m)
1	5	Element 99	166.5
2	10	Element 99	166.5
3	5	Element 99; Element 136	166.5; 221.5
4	10	Element 99; Element 136	166.5; 221.5

4.2 Analysis of the results of data fusion

4.2.1 Single-indicator data fusion analysis

(1) Data fusion analysis based on modal indicators.

In many testing environments, owing to the limitations of on-site conditions and sensor types, only a single indicator can be measured, such as in certain specific bridges that can only provide modal data. When only modal data are available, the curvature and displacement mode differences can be derived by using the aforementioned method. We combined these two indicators according to D–S evidence theory. From the perspectives of excitation components, excitation energy, and damping dissipation, structural vibrations are predominantly characterized by low-order modes, and the acquisition of higher-order components is challenging in practice. Therefore, it is considered appropriate to utilize first-order data for analysis and computation.

The data fusion results are shown in Fig. 6. We found that the data fusion algorithm could clearly identify the location of the damage. Regardless of whether there were one or two points of damage, the waveform in the damaged area was significantly larger than that at other locations. To further analyze the improvements in the damage detection performance as a result of data fusion, the sub-peak-to-peak ratio of the curvature modes before fusion and that of the fusion indicators after fusion were extracted, as detailed in Table 3.

By analyzing the sub-peak-to-peak ratio before and after fusion, we were able to draw the following conclusions. The sub-peak-to-peak ratio when using the fusion index as the identification index was lower than the sub-peak-to-peak ratio calculated by applying the curvature mode as the damage index. The reduction in single damage points was significant, ranging from 12% to 48%, whereas the reduction in two concurrent damage points was approximately 2%. Therefore, the superiority of the fused indicators can be intuitively demonstrated by observing Fig. 6. Quantitative analysis based on the data from Table 3 also demonstrates the superiority of fused indicators over a single indicator during damage detection.

(2) Data fusion analysis based on moving load excitation response.

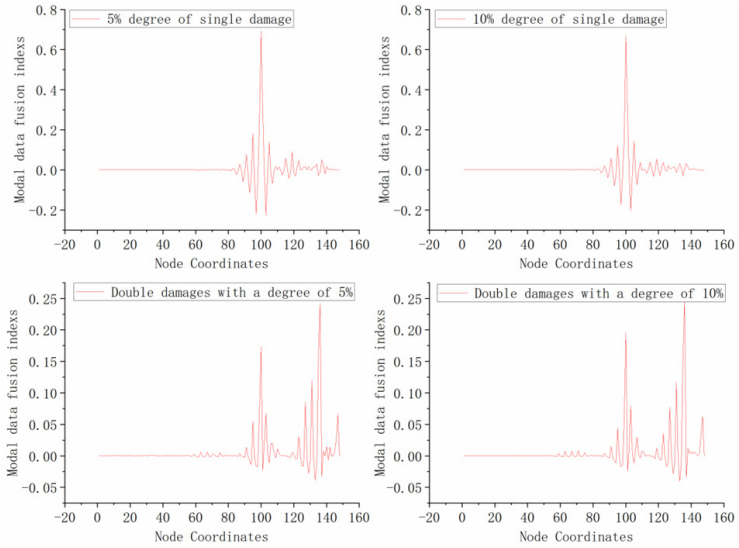

Fig. 6 Modal-based multivariate data fusion results

Table 3 Modal indicator sub-peak and peak results

Working condition	Curvature mode sub-peak	Curvature mode peak value	Sub-peak of fusion indicators	Peak value of fusion indicators	Curvature mode sub-peak-to-peak ratio	Sub-peak-to-peak ratio of fusion indicators	Reduction
1	1.20×10^{-5}	2.50×10^{-5}	0.181	0.692	0.480	0.261	45.6%
2	2.30×10^{-5}	5.50×10^{-5}	0.144	0.669	0.418	0.216	48.3%
3	9.00×10^{-6}	2.50×10^{-5}	0.055	0.173	0.360	0.316	12.2%
	1.50×10^{-5}	3.00×10^{-5}	0.120	0.242	0.500	0.495	1%
4	2.30×10^{-5}	5.50×10^{-5}	0.079	0.195	0.418	0.405	3.1%
	2.60×10^{-5}	6.20×10^{-5}	0.100	0.244	0.419	0.412	1.7%

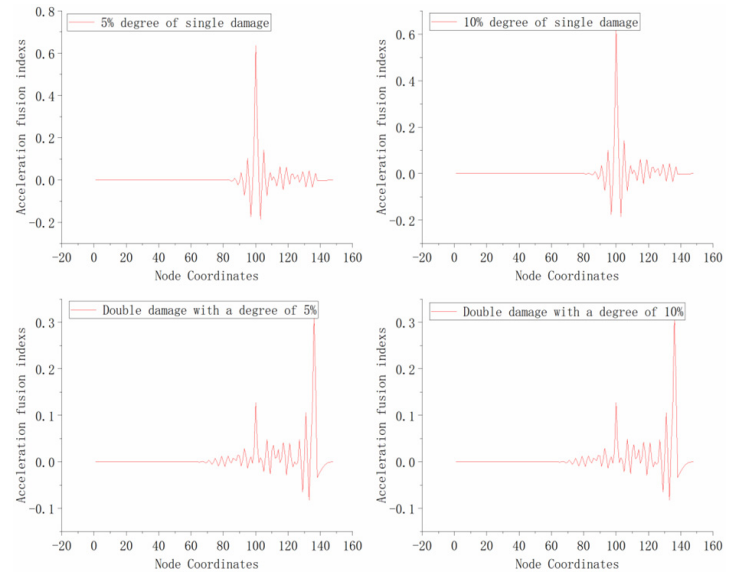

Fig. 7 Multivariate data fusion results based on the moving load excitation response

Only response data based on the moving load excitation were analyzed. The acceleration energy and acceleration energy curvature differences were determined based on the methods in Section 3.2. These two indicators were integrated into the data. The detection results are shown in Fig. 7.

Following fusion of the response indicators based on moving load excitation, the waveform associated with the

Table 4 Moving load excitation sub-peak and peak results

Working condition	Acceleration energy curvature sub-peak	Acceleration energy curvature peak value	Sub-peak of fusion indicators	Peak value of fusion indicators	Acceleration energy curvature sub-peak-to-peak ratio	Sub-peak-to-peak ratio of fusion indicators	Reduction
1	0.093	0.221	0.142	0.636	0.419	0.224	46.5%
2	0.093	0.221	0.143	0.633	0.419	0.225	46.3%
3	0.063	0.217	0.024	0.127	0.290	0.190	34.5%
	0.081	0.160	0.106	0.309	0.507	0.344	32.2%
4	0.130	0.459	0.029	0.127	0.284	0.229	19.4%
	0.169	0.338	0.105	0.310	0.500	0.339	32.2%

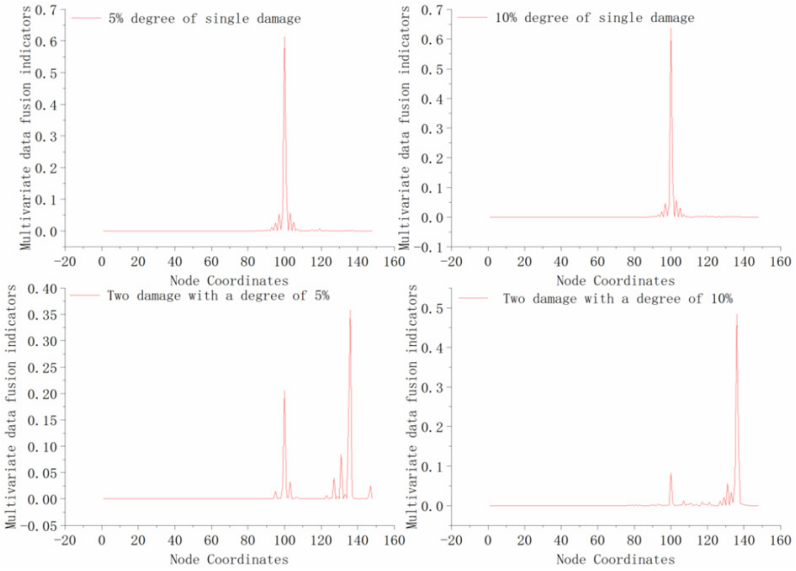

Fig. 8 Results of multivariate indicator data fusion identification

damaged area was found to exhibit more fluctuation than the waveform associated with the undamaged area. To analyze the effect of fusion on damage detection, the sub-peak-to-peak ratios of the curvature modes before fusion and the indicators after fusion were extracted separately. The results are listed in Table 4.

By analyzing the sub-peak-to-peak ratio before and after fusion, we were able to draw the following conclusions. The sub-peak-to-peak ratio of the fusion index was lower than that calculated by using the single-damage index. Regardless of whether there was a single point of damage or two points of damage, the decrease in the sub-peak-to-peak ratio was significant. This decrease ranged between 19% and 46%. Considering the decrease in the sub-peak-to-peak ratio, the fusion index has certain advantages over a single index in the detection process.

4.2.2 Fusion analysis for multiple indicators

To increase the damage detection accuracy, the damage indicators were fused from different systems based on the data treated with D–S evidence theory. Secondary fusion was performed between the modal fusion indicators and moving load excitation fusion indicators. The detection results are shown in Fig. 8.

This can be inferred from the data fusion results for the multiple indicators. With the exception of the sharp convexity of the waveform associated with the damaged element, the fluctuations in the other elements tended to be nonexistent. As the degree of damage increased, the number of extreme points in the damage detection graph also increased. The waveform fluctuations near the damaged element were very small. Therefore, the method of applying multiple fusions is highly beneficial for damage detection and less prone to damage misjudgment.

The detection performance before and after secondary fusion was also compared. The sub-peak-to-peak ratios of the damage indicators before and after secondary fusion were extracted, as shown in Table 5.

The sub-peak-to-peak ratio of the secondary fusion index was lower than that of the single-index fusion, regardless of whether there were one or two points of damage. The peak-to-peak ratio decreased significantly within a range of 16% to 99%. The decrease in the sub-peak-to-peak ratio indicates that the multivariate data fusion index significantly improved detection performance relative to the modal data fusion index. Therefore, we believe that multivariate data fusion indicators have certain advantages in damage detection.

Table 5 Multiple-indicator sub-peak and peak results

Working condition	Multiple fusion indicator sub-peak	Peak value of multiple fusion indicators	Sub-peak-to-peak ratio of fusion indicators	Reduction (vs. Table 3)	Reduction (vs. Table 4)
1	0.054	0.614	0.087	66.67%	61.16%
2	0.057	0.637	0.090	58.33%	60.00%
3	0.033	0.205	0.159	49.68%	16.32%
	0.085	0.359	0.236	52.32%	31.40%
4	0.00014	0.0817	0.002	99.51%	99.13%
	0.034	0.484	0.070	83.01%	79.35%

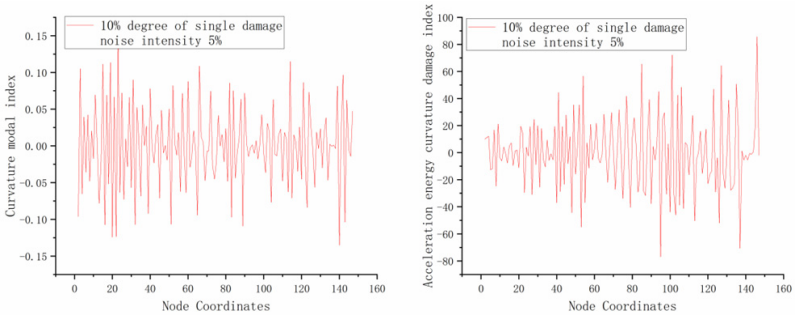

Fig. 9 The 10% level of single damage accompanied by noise

5. Robustness analysis

In real environments, noise is often not generated by a single source but rather by a complex combination of noises from different sources (Desjardins and Lau 2022). Actual noise can be considered as a superposition of random variables with different probability distributions. These random variables are independent, according to the central limit theorem. The normalization of these random variables tends toward a Gaussian distribution as the number of random variables increases. Based on this assumption, the use of Gaussian white noise can better simulate actual unknown noise.

A signal with noise can be represented by Eq. (16)

$$y_{d,noise} = y_d + E_p N_{noise} \sigma(y_d) \tag{16}$$

where $y_{d,noise}$ is the dynamic response with noise; y_d is the dynamic response in the absence of noise; E_p denotes the noise level, N_{noise} is a random sequence with a mean of 0 and standard deviation of 1; $\sigma(y_d)$ is the standard deviation of the dynamic response in the absence of noise.

Noise intensities of 5, 10, 20, and 30% were added to the sampled signals, which included modal indicators and data on moving load excitation response. Matlab was used as the platform for calculations.

The typical simulated conditions with added random noise were subjected to computational analysis. Only the scenario with a noise intensity of 5% (Condition 2) is presented, where modal indicators and vibration indicators of vehicle excitation were calculated separately. The specific details are illustrated in Fig. 9.

From the analysis of Fig. 9, it is evident that without noise processing, the damage identification method fails to detect the damage. Therefore, it is necessary to apply the theory mentioned in Section 2.1 to preprocess the response data for noise reduction.

To determine whether damage had occurred, the damage warning line was calculated based on the collected response data. The applied formulas are shown in Eqs. (17) and (18) (Wang 2017).

$$DI_k > \frac{S}{N}\sum_{i=1}^{N} DI_i \tag{17}$$

$$S\frac{DI_{max}}{\frac{1}{N}\sum_{i=1}^{N} DI_{i_{min_{max}}}} \tag{18}$$

where DI_i is the damage index constructed by using the dynamic response of the i-th beam, DI_{max} is the maximum value of the damage index for each element of the beam segment, N is the total number of cable-stayed bridge segments, and S is the safety factor. Given that $DI_k > \frac{S}{N}\sum_{i=1}^{N} DI_i$, we believe that damage occurred in the k-th element. Because of the smaller S value, the discrimination criteria were more conservative. The S value in this study was taken as the mean of the S values.

Regarding the single-damage results for minor (i.e., 5%) damage occurring in Element 99, as the noise level increased, all four sets of data fusion detection results indicated damage at the position of Element 99 (Fig. 10). The peak of each waveform was found to be higher than the predetermined damage threshold value. When the noise intensity level did not exceed 20%, using data fusion

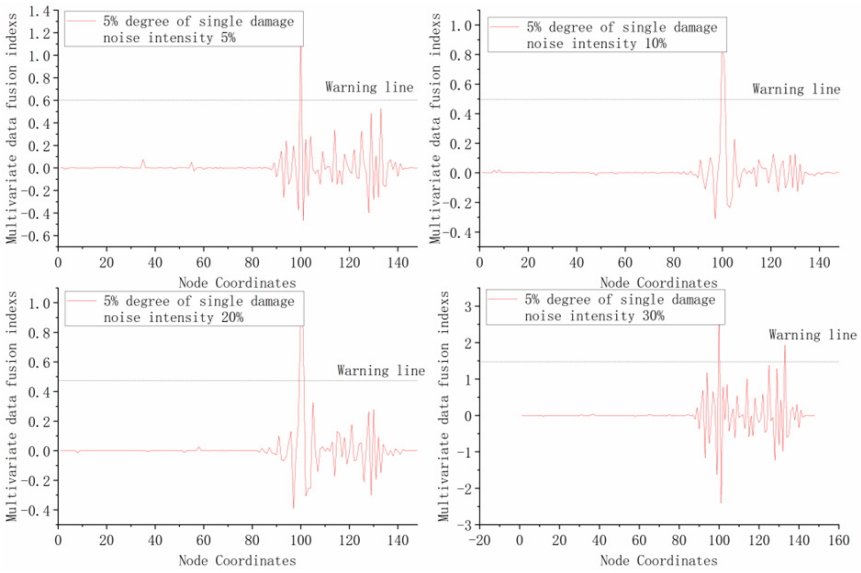

Fig. 10 Damage detection results for single-point 5% damage

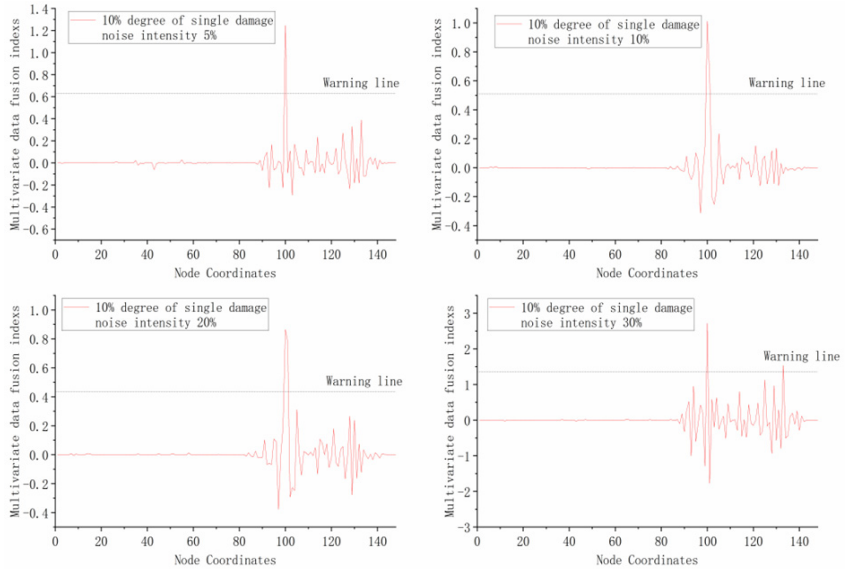

Fig. 11 Damage detection results for single-point 10% damage

indicators resulted in effective damage detection. Additionally, the magnitude of the waveform fluctuations decreased with distance from the damaged element. We observed significant fluctuations near the damaged element, but the damage threshold was not exceeded. However, when the noise intensity level reached 30%, the peak for Elements 99 and 133 exceeded the damage threshold. Therefore, we believe that, when the noise intensity level reaches 30%, anomalies will be observed in single-damage detection results.

We subjected Element 99 to a 10% level of damage; the results are shown in Fig. 11. As the noise increased, all four conditions of data fusion detection resulted indicated damage at Element 99. The overall trend was consistent with the results of the 5% level of single-point damage. Regardless of the extent of damage, the data fusion indicators were able to effectively detect damage up to a noise intensity level of 20%. Additionally, the magnitude of the waveform fluctuations steadily decreased with distance from the damaged element. There was significant fluctuation near the damaged element, but the corresponding value did not exceed the damage threshold. This can be observed by comparing the single-damage condition with a 5% degree. As the extent of damage increased, the waveform became relatively pure, which conformed to the rule indicating that a higher degree of damage corresponds to more accurate detection. However, when the noise intensity level reached 30%, the level of damage increased from 5% to 10%. Furthermore, the waveform peaks of Elements 99 and 133 exceeded the damage threshold. Therefore, when the noise level was too high and the intensity reached 30%, the single-damage detection result appeared to be abnormal. However, at the 5% level of damage, the difference between the peak of the

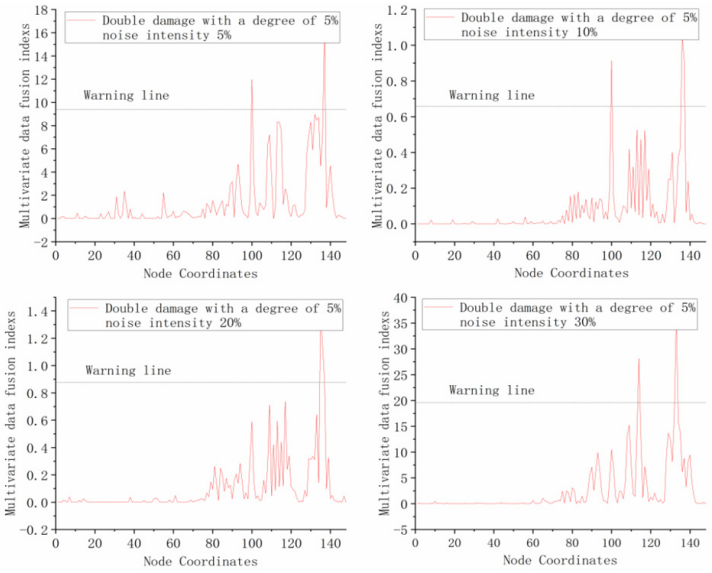

Fig. 12 Damage detection results for multi-point 5% damage

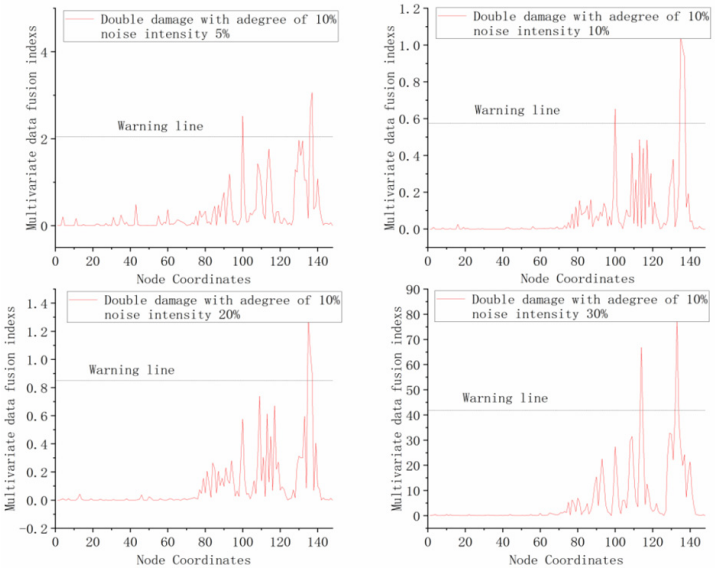

Fig. 13 Damage detection results for multi-point 10% damage

anomaly and the threshold was relatively small.

Elements 99 and 136 of the bridge were subjected to concurrent minor damage to a degree of 5%. As shown in Fig. 9, at a noise intensity level up to 10%, the multimodal method could effectively identify minor damage. This is confirmed by Fig. 12, as one can see that only the extreme peaks of the waveform, which corresponded to the two damaged elements (i.e., Elements 99 and 136), exceeded the damage threshold. Although there were smaller peaks, which indicated other undamaged elements, as shown in the figure, their highest values were below the damage threshold. When the noise intensity level reached 20%, only the peak associated with Element 136 exceeded the threshold; thus, the damage to Element 99 was not detected. This indicates that, when the structure suffers multiple points of minor damage, the detection results are more susceptible to noise than in the case of a single point of damage. At a noise level of 30%, the waveform peak associated with Element 133 exceeded the damage threshold, as did that corresponding to a position near Element 113. Furthermore, according to the detection results, Element 99 suffered no significant level of damage when the noise intensity level was 30%, as the damage threshold was not exceeded. Therefore, when the noise reached 30%, the damage detection result was misjudged, indicating that the damage detection method was ineffective.

The results of simulating a 10% level of damage in Elements 99 and 136 are shown in Fig. 13. Up to a noise intensity level of 10%, the data fusion detection method could effectively detect damage. However, when the noise intensity level increased to 20%, only the peak corresponding to Element 136 exceeded the damage threshold, indicating that the damage to Element 99 was not

detected. When the noise intensity level increased to 30%, the peak corresponding to Element 133 exceeded the threshold, as did the peak corresponding to a point near Element 113, which was not damaged. Moreover, the peak corresponding to Element 99 did not exceed the threshold. This indicates that, when the noise intensity level reaches 30%, there is a misjudgment in the multi-damage detection results. Thus, the damage detection method is ineffective.

6. Conclusions

This paper describes a data-fusion damage detection method for bridges that is based on statistical dimensionality and noise reduction. This method entails applying D–S evidence theory to fuse modal indicators with moving load excitation response indicators to develop a new set of damage indicators. Statistical analysis techniques were used to denoise the response data and thus effectively identify single-point and two-point damage in cable-stayed bridges. The effectiveness of the method was verified via finite-element simulations, and the following conclusions were drawn:

- This method can effectively denoise the data and, to some extent, eliminate the influence of noise in the damage detection process. Data fusion can effectively increase detection accuracy when a single damage indicator is used for identification.
- When a structure has a single point of damage, the noise intensity level should not exceed 20%. When the extent of damage was small (i.e., only 5%), the proposed method could accurately identify the location of the damage. When the noise intensity level reached 30%, damage could not be accurately detected, indicating that the proposed method is not robust against excessive noise levels.
- We also simulated two points of structural damage. When the noise intensity level did not exceed 10%, the proposed method was able to accurately identify the two points of damage even when the extent of damage was small (i.e., only 5%). However, when the noise intensity level reached 20%, only one of the two points of damage was detected. Furthermore, when the noise intensity level reached 30%, only one point of damage was detected, and an undamaged element was incorrectly indicated to have suffered damage. To ensure high detection accuracy, the proposed method demonstrates effectiveness at noise intensity levels up to 10% when detecting two damage points.
- It is worth noting that the vehicle-induced vibration response in this paper comes from simulating the single vehicle effect in FEA. Therefore, research on multi-vehicle incentive response or random vehicle condition incentive response is needed in the future.

Data availability

The data used to support the findings of this study have been included in this article.

Conflicts of interest

The authors confirm that the funding received did not lead to any conflict of interest regarding the publication of this manuscript.

Funding statement

The authors disclose receipt of the following financial support for the research, authorship, and/or publication of this article: This work was supported by the National Key R&D Program of China (2018YFC0809606 and 2018YFC0809600) and the Shenyang Science and Technology Plan Project Fund (23-407-3-19).

Author contributions

Yue Cao: Writing – original draft, Supervision, Investigation, Funding acquisition, Conceptualization. Long-Sheng Bao: Writing – original draft, Validation, Investigation, Data curation. Xiao-Wei Zhang: Writing – review & editing, Validation, Supervision, Investigation, Funding acquisition, Conceptualization. Zhang-Fei Wang: Writing – review & editing, Funding.

References

AlMutawa, J. (2007), "Identification of errors-in-variables model with observation outliers based on Minimum-Covariance-Determinant", In: *American Control Conference*, pp. 134-139. http://doi.org/10.1109/acc.2007.4282931

Bai, R.B., Xu, Z.M. and Zhang, J.B. (2017), "Damage detection for plate-like structures based on DT-CWT denoising and fusion of Katz's fractal dimension trajectories", *J. Vib. Shock*, **36**(5), 87-94. http://doi.org/10.13465/j.cnki.jvs.2017.05.014

Barros, B., Conde, B., Cabaleiro, M. and Riveiro, B. (2023), "Design and testing of a decision tree algorithm for early failure detection in steel truss bridges", *Eng. Struct.*, **289**, 1-19. http://doi.org/10.1016/j.engstruct.2023.116243

Bin, Z., Zhen, Z., Jun, Z. and Qing, X. (2016), "Damage identification analysis of truss string structure based on modal parameters", *J. Build. Struct.* http://doi.org/10.14006/j.jzjgxb.2016.S1.019

Chakrabarty, S., Thiergart, O. and Habets, E.A. (2015), "A Bayesian approach to spatial filtering and diffuse power estimation for joint dereverberation and noise reduction", In: *IEEE International Conference on Acoustics, Speech and Signal Processing* (*ICASSP*), pp. 753-757. http://doi.org/10.1109/ICASSP.2015.7178070.

Daneshvar, M.H., Saffarian, M., Jahangir, H. and Sarmadi, H. (2023), "Damage identification of structural systems by modal strain energy and an optimization-based iterative regularization method", *Eng. Comput.*, **39**, 2067-2087. http://doi.org/10.1007/s00366-021-01567-5

Desjardins, S. and Lau, D. (2022), "Advances in intelligent long-term vibration-based structural health-monitoring systems for bridges", *Adv. Struct. Eng.*, **25**(7), 1413-1430. https://doi.org/10.1177/13694332221081186

Desjardins, S.L. and Lau, D.T. (2024), "Enhanced operational modal analysis and change point detection for vibration-based structural health monitoring of bridges", *J. Infrastr. Intell. Resil.*, **3**(4), 100-121.

https://doi.org/10.1016/j.iintel.2024.100121
Fathi, A. and Naghsh-Nilchi, A.R. (2012), "Efficient image denoising method based on a new adaptive wavelet packet thresholding function", *IEEE Transact*. *Image Process*., **21**, 3981-3990. http://doi.org/10.1109/TIP.2012.2200491
Huang, B. and Chen, H. (2019), "A new approach for stochastic model updating using the hybrid perturbation-Garlekin method", *Mech*. *Syst*. *Signal Process*., **129**, 1-19. http://doi.org/10.1016/j.ymssp.2019.04.012
Jamshidi, M. and El-Badry, M. (2023), "Structural damage severity classification from time-frequency acceleration data using convolutional neural networks", *Structures*, **54**, 236-253. https://doi.org/10.1016/j.istruc.2023.05.009
Li, S.L., Shi, C.P., Wu, G.M., Hou, S.T., Wang, C., Wang, T.G. and Jiang, N. (2024), "Distribution characteristics and prediction method of tire–road AE noise in the monitoring of prestressed hollow slab bridges", *Measurement*, **227**, p. 114211. https://doi.org/10.1016/j.measurement.2024.114211
Liu, X.J., Xiang, L. and Zhang, S.X. (2015), "Damage identification of simply supported beam bridges based on wavelet analysis", *J*. *Vib*. *Measure*. *Diagnos*., **35**(5), 866-872. http://doi.org/10.16450/j.cnki.issn.1004-6801.2015.05.010
Liu, G.Y., Liu, X.J. and Zhang, S.X. (2021), "Damage identification and analysis of simply supported beam bridges based on lifting wavelet transform and statistical theory", *J*. *Disaster Prevent*. *Mitigat*. *Eng*., **41**(3), 594-602. https://doi.org/10.13409/j.cnki.jdpme.201904047
Mekjavić, I. (2013), "Damage identification of bridges from vibration frequencies", *Tehnički vjesnik*, **20**, 155-160. http://doi.org/10.1061/(ASCE)MT.1943-5533.0000604
Moschas, F., Psimoulis, P.A. and Stiros, S.C. (2013), "GPS/RTS data fusion to overcome signal deficiencies in certain bridge dynamic monitoring projects", *Smart Struct*. *Syst*., *Int*. *J*., **12**(3-4), 251-269. http://doi.org/10.12989/sss.2013.12.3_4.251
Reynders, E., Roeck, G.D., Gundes Bakir, P. and Sauvage, C. (2007), "Damage identification on the tilff bridge by vibration monitoring using optical fiber strain sensors", *J*. *Eng*. *Mech*., **133**, 185-193. http://doi.org/10.1061/(ASCE)0733-9399(2007)133:2(185)
Seyedpoor, S.M. and Yazdanpanah, O. (2014), "An efficient indicator for structural damage localization using the change of strain energy based on static noisy data", *Appl*. *Mathe*. *Modell*., **38**, 2661-2672. http://doi.org/10.1016/j.apm.2013.10.072
Shelley, T.J. and Liew, C.K. (2013), "Application of wavelet parameters for impact damage detection in plates", *Key Eng Mater*., **558**, 12-24. http://doi.org/10.4028/www.scientific.net/KEM.558.12
Sohn, H. and Law, K.H. (2015), "Bayesian probabilistic damage detection of a reinforced-concrete bridge column", *Earthq*. *Eng*. *Struct*. *Dyn*., **29**, 1131-1152. http://doi.org/10.1002/1096-9845(200008)29:8<1131::AID-EQE959>3.0.CO;2-J
Sousa Tomé, E., Pimentel, M. and Figueiras, J. (2019), "Online early damage detection and localisation using multivariate data analysis: application to a cable-stayed bridge", *Struct*. *Control Health Monitor*., **26**(11), p. e2434. http://doi.org/10.1002/stc.2434
Torbol, M., Kim, S. and Shinozuka, M. (2013), "Long term monitoring of a cable stayed bridge using duramote", *Smart Struct*. *Syst*., *Int*. *J*., **11**(5), 453-476. http://doi.org/10.12989/sss.2013.11.5.453
Shi, Q., Qian, S., Luo, Z., Cao, Z., Yang, C., Hu, K. and Han, W. (2024), "Uncertain damage identification methods based on residual force vector under the influence of measurement noise", *Int*. *J*. *Non-Linear Mech*., **163**, p. 104732. https://doi.org/10.1016/j.ijnonlinmec.2024.104732
Wang, X.C. (2017), "Research on damage identification method of simply supported beams based on lifting wavelet transform", Master's Thesis; Tianjin University, Tianjin, China. [In Chinese]
Wang, S., Chen, Y. and Zhang, L. (2019), "Fusion of multiple damage indices for structural health monitoring using Dempster-Shafer evidence theory", *Mech*. *Syst*. *Signal Process*., **123**, 456-467.
Wang, Z., Yang, D.H., Yi, T.H., Zhang, G.H. and Han, J.G. (2022), "Eliminating environmental and operational effects on structural modal frequency: A comprehensive review", *Struct*. *Control Health Monitor*., **29**(11), 1-24. https://doi.org/10.1002/stc.3073
Yıldırım, U. (2023), "Influence of asphalt removal on operational modal analysis of Egebækvej Bridge", *Smart Struct*. *Syst*., *Int*. *J*., **31**(1), 171-181. http://doi.org/10.12989/sss.2023.31.1.171
Hosseinzadeh, A.Z., Ghodrati Amiri, G. and Koo, K.Y. (2016), "Optimization-based method for structural damage localization and quantification by means of static displacements computed by flexibility matrix", *Eng*. *Optimiz*., **48**, 543-561. http://doi.org/10.1080/0305215X.2015.1017476
Zhang, J., Yi, T.H., Qu, C.X., Han, Q., Wang, Y.F. and Mei, X.D. (2023), "Experimental studies of extracting bridge mode shapes by response of a moving vehicle", *J*. *Bridge Eng*., **28**, p. 04023076. https://doi.org/10.1061/JBENF2.BEENG-6243